Materials Advances

ROYAL SOCIETY OF CHEMISTRY

COMMUNICATION

View Article Online
View Journal | View Issue

Check for updates

Cite this: *Mater. Adv.*, 2026, 7, 192

Received 14th October 2025,
Accepted 10th December 2025

DOI: 10.1039/d5ma01185j

rsc.li/materials-advances

Open Access Article. Published on 17 December 2025. Downloaded on 4/2/2026 1:22:20 PM.
This article is licensed under a Creative Commons Attribution 3.0 Unported Licence.

# Mitigation of mechanical degradation in silicon thin-film anodes *via* delithiation cut-off voltage control

Y. Eto,[a] K. Nozawa,*[a] T. Suemasu[a] and K. Toko *[ab]

**Silicon (Si) is a high-capacity anode material for lithium-ion batteries; however, its large volume change during cycling causes severe mechanical degradation. We show that optimizing the delithiation cut-off voltage effectively suppresses interfacial delamination in Si thin-film anodes. By limiting delithiation at 0.6 V, partial Li retention reduces interfacial stress and prevents structural collapse, achieving 92% capacity retention (2200 mAh $g^{-1}$) after 100 cycles. Cross-sectional analyses confirmed suppressed shrinkage and strong adhesion to the substrate. This simple voltage-control strategy provides a universal and practical route to enhance the durability of Si-based and other alloy-type anodes.**

Rechargeable lithium-ion batteries (LIBs) are essential energy storage systems that power portable electronics, electric vehicles, and renewable energy infrastructures.[1–3] Their high energy density and long cycle life have supported rapid technological advances. However, the performance of current LIBs—based on graphite anodes and layered oxide cathodes—has nearly reached its theoretical limit.[4,5] To further improve energy density and durability, new electrode materials capable of storing larger amounts of lithium while maintaining structural stability are required. In pursuit of higher-capacity materials, alloy- and conversion-type anodes have been extensively studied, among which silicon (Si) stands out because of its high theoretical capacity (3579 mAh $g^{-1}$ for $Li_{15}Si_4$), natural abundance, and environmental benignity.[6–8]

Despite its advantages, Si suffers from drastic volume changes of up to 400% during lithiation and delithiation, leading to cracking, pulverization, and delamination from the current collector.[9,10] These mechanical failures disrupt electron transport and destabilize the solid–electrolyte interphase (SEI), resulting in severe capacity fading. To mitigate these problems, various approaches—such as nanostructuring,[11–16] composite formation with conductive matrices,[17–20] and artificial SEI coatings[21–24] have been proposed. While these strategies partially suppress mechanical degradation, they often involve complex fabrication processes or compromise the volumetric energy density. In addition to material design, electrochemical factors such as the potential window also strongly influence the degradation behavior of Si anodes.[25–27] Complete delithiation at low potentials enhances interfacial stress and accelerates SEI fracture, whereas limiting the delithiation voltage range within the Si–Li reaction potential can moderate volume changes and improve cycling stability. Several studies have explored the voltage window for Si-based electrodes; however, most examined composite Si electrodes,[28] full- or deep-delithiation behavior,[29] or lower cut-off regulation.[30] Recent work on alloy-type anodes also focused mainly on SEI suppression rather than delithiation control.[31] For Si thin films, only limited efforts have addressed cut-off voltages and no systematic study has intentionally varied the delithiation cut-off voltage to control delithiation-induced shrinkage.

In this study, we focus on the delithiation cut-off voltage as a new perspective for addressing the intrinsic challenges of Si anodes. By optimizing the delithiation voltage, lithium ions were partially retained within the Si layer instead of being completely extracted, effectively mitigating the structural damage associated with repeated lithiation and delithiation. This simple voltage-control strategy achieved outstanding electrochemical performance, with a discharge capacity of approximately 2200 mAh $g^{-1}$ and 92% capacity retention after 100 cycles. These results demonstrate that appropriate delithiation cut-off voltage regulation can suppress interfacial delamination, improve mechanical stability, and extend the lifetime of Si thin-film anodes, offering a practical route toward high-capacity and durable lithium-ion batteries.

To investigate the effect of delithiation cut-off voltage on the electrochemical and structural properties of Si thin-film anodes, samples were prepared by radio-frequency (RF) magnetron sputtering. A 250 nm thick amorphous Si layer was

[a] *Institute of Applied Physics, University of Tsukuba, 1-1-1 Tennodai, Tsukuba, Ibaraki, 305-8573, Japan. E-mail: nozawa.koki.td@alumni.tsukuba.ac.jp, toko@bk.tsukuba.ac.jp*

[b] *Tsukuba Institute for Advanced Research (TIAR), University of Tsukuba, 1-1-1 Tennodai, Tsukuba, Ibaraki, 305-8577, Japan*



© 2026 The Author(s). Published by the Royal Society of Chemistry

Open Access Article. Published on 17 December 2025. Downloaded on 4/2/2026 1:22:20 PM.
This article is licensed under a Creative Commons Attribution 3.0 Unported Licence.

deposited onto molybdenum (Mo) foil (99.95% purity, 50 μm thickness) using a sputtering system (Sanyu Electron SVC-700RF) with an argon plasma atmosphere. Mo foil was selected as the substrate because sputtered Si films are known to exhibit stronger adhesion on Mo than on Cu, which frequently suffers from early delamination during cycling.[32–34] In addition, Mo provides a higher in-plane stiffness (Young's modulus ≈ 330 GPa) than Cu (≈ 110 GPa), offering a larger lateral constraint against shrinkage-induced peeling of the Si layer. The base pressure was maintained at $3.0 \times 10^{-4}$ Pa, and the RF power was set to 50 W, corresponding to a deposition rate of approximately 6.4 nm $min^{-1}$. The purity of the Si target was 99.9%. After deposition, the films were punched into 10 mm diameter disks and dried under vacuum at 120 °C for 12 h prior to cell assembly. Coin-type cells (CR2032) were fabricated in an argon-filled glove box (UNICO UL-Ef1000A-TKSP) using the Si thin-film as the working electrode, lithium metal foil as the counter and reference electrode, and a polypropylene separator (Celgard 2400). The electrolyte was a 1 mol $L^{-1}$ solution of lithium hexafluorophosphate ($LiPF_6$) dissolved in ethylene carbonate (EC) and diethyl carbonate (DEC) with a volume ratio of 1 : 1. Galvanostatic charge/discharge measurements were carried out using an electrochemical analyzer (Meiden Hokuto HJ1001SD8). The lithiation cut-off voltage was fixed at 0.005 V for all samples, while the delithiation cut-off voltages ($V_d$) were varied at 2.0, 0.8, 0.6, and 0.4 V to control the degree of delithiation. For each voltage condition, three-coin cells were prepared and tested to confirm reproducibility. The value of 2.0 V was used as a fully delithiated reference, whereas the three lower voltages were selected to regulate the extent of Li extraction within the practical Si–Li reaction window. Motivated by the well-documented delithiation potentials of amorphous Si (≈ 0.3–0.5 V),[9] we selected 0.4, 0.6, and 0.8 V as representative cut-off voltages to systematically tune the degree of delithiation. Specifically, 0.4 V lies near the lower boundary of the delithiation plateau and leaves a relatively Li-rich a-$Li_xSi$ phase; 0.6 V is slightly above the upper delithiation peak and corresponds to intermediate Li content; and 0.8 V exceeds the main alloying potentials, approaching nearly complete delithiation while remaining within a practically meaningful window. After electrochemical testing, the cells were disassembled using a coin-type cell separator (Hohsen) to examine the Si anode morphology. Surface and cross-sectional structures were analyzed by scanning electron microscopy (SEM, Hitachi High-Technologies SU-7000) equipped with an energy-dispersive X-ray spectrometer (EDX, Oxford AZtec). Transmission electron microscopy (TEM) and high-angle annular dark-field scanning TEM (HAADF-STEM) observations were performed using a field-emission TEM (HF5000, 200 kV) equipped with an EDX detector to analyze interfacial structures and elemental distributions. Focused ion beam (FIB) cross-sectioning was conducted using a Helios Nanolab 600i system. For SEM/EDX surface observations, the extracted electrodes were gently rinsed with deionized water to remove residual electrolyte ($LiPF_6$) and subsequently dried under $N_2$ flow. In contrast, for FIB-SEM and TEM cross-sectional analyses, the Si films were in a lithiated state; therefore, they were not rinsed but gently dried under $N_2$ flow to avoid structural disturbance. As a result, a thin layer of $LiPF_6$-derived residue remained on the Si surface. For cross-sectional analysis, a Pt protective layer was deposited on the sample surface prior to FIB milling to prevent damage and redeposition during Ga ion irradiation.

Fig. 1(a)–(d) shows the galvanostatic charge/discharge curves of the Si thin-film anodes measured at $V_d$ of 2.0, 0.8, 0.6, and 0.4 V. The measurements were performed at 1C for 200 cycles. All samples exhibited distinct charge/discharge behavior throughout the cycling test. The plateau region observed around 0.2 V corresponds to Li-ion insertion and extraction into and from the Si layer. For the 0.4 and 0.6 V samples, where the discharge was terminated within the Si–Li reaction range, the plateau region ended earlier and became shorter. The first-cycle charge capacities exceeded 3000 mAh $g^{-1}$ for all samples with negligible variation, whereas the first discharge capacities decreased with decreasing $V_d$. This is attributed to incomplete delithiation because lower $V_d$ lies within the delithiation potential region, leaving part of the Li ions in the Si layer. Fig. 1(e) summarizes the discharge capacity as a function of cycle number. In all samples, small cycle-to-cycle fluctuations

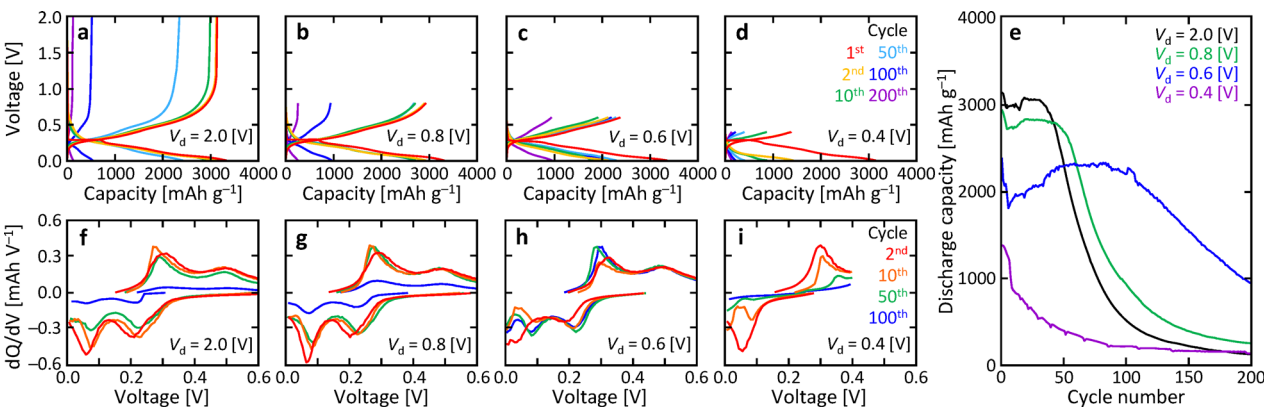


Fig. 1 Delithiation cut-off voltage ($V_d$) dependence of the anode properties. (a)–(d) Galvanostatic charge/discharge cycles at $V_d$ = (a) 2.0 V, (b) 0.8 V, (c) 0.6 V, and (d) 0.4 V. (e) Cycle dependence of discharge capacities. (f)–(i) d$Q$/d$V$ plots at $V_d$ = (f) 2.0 V, (g) 0.8 V, (h) 0.6 V, and (i) 0.4 V.

Open Access Article. Published on 17 December 2025. Downloaded on 4/2/2026 1:22:20 PM.
This article is licensed under a Creative Commons Attribution 3.0 Unported Licence.

appeared during the early stages of cycling, which are commonly reported for Si anodes and mainly arise from repeated SEI fracture/reformation and the exposure of fresh Si surfaces caused by crack generation. Subsequently, the capacity gradually decreased with cycling, reflecting the typical degradation behavior caused by the expansion and contraction of the Si layer during lithiation and delithiation.[35,36] The extent of capacity fading varied with $V_d$. The 2.0 V sample exhibited a steep capacity drop after approximately 40 cycles, and its capacity decreased to 520 mAh $g^{-1}$ ($\approx$ 16% of the initial value) after 100 cycles. In contrast, the 0.8 and 0.6 V samples exhibited smaller initial capacities but maintained higher capacities for longer cycles. Particularly, the 0.6 V sample retained approximately 2200 mAh $g^{-1}$ (92% of the initial capacity) after 100 cycles, demonstrating excellent capacity retention and gradual fading. Interestingly, this sample also exhibited a slight capacity increase during the early cycles, which was reproducibly observed in all cells cycled at 0.6 V. We infer that, under this condition, partial delithiation suppresses catastrophic interfacial delamination so that the Si film remains anchored to the Mo substrate; with repeated cycling, fine surface cracks then develop mainly near the film surface (as discussed later in Fig. 2 and 3), exposing previously inactive Si to the electrolyte and gradually enlarging the electrochemically accessible area. Although SEI reformation on these newly exposed surfaces and other degradation processes eventually lead to capacity fading at longer cycle numbers, the net effect in the early stages is a modest increase in reversible capacity. The 0.4 V sample, however, exhibited both a small initial capacity and a rapid capacity decrease, suggesting that insufficient delithiation caused Li accumulation within the Si, leading to degradation. The differential capacity ($dQ/dV$) plots shown in Fig. 1(f)–(i) exhibit broad peaks at approximately 0.1 and 0.25 V during lithiation and 0.3 and 0.5 V during delithiation, corresponding to Li insertion/extraction in amorphous Si.[37–40] Because amorphous Si does not undergo sharp phase transitions as crystalline Si does, the peaks appear broader.[41] A more detailed interpretation of the $dQ/dV$ behavior further clarifies the voltage-dependent degradation mechanisms. According to previous studies on Si–Li alloying reactions, the peak positions, widths, and shifts in $dQ/dV$ curves reflect changes in the local a-$Li_xSi$ structure and the degree of cell polarization.[42,43] For the 2.0 V sample, the peak intensities decrease markedly with cycling, indicating substantial degradation of the active Si layer.

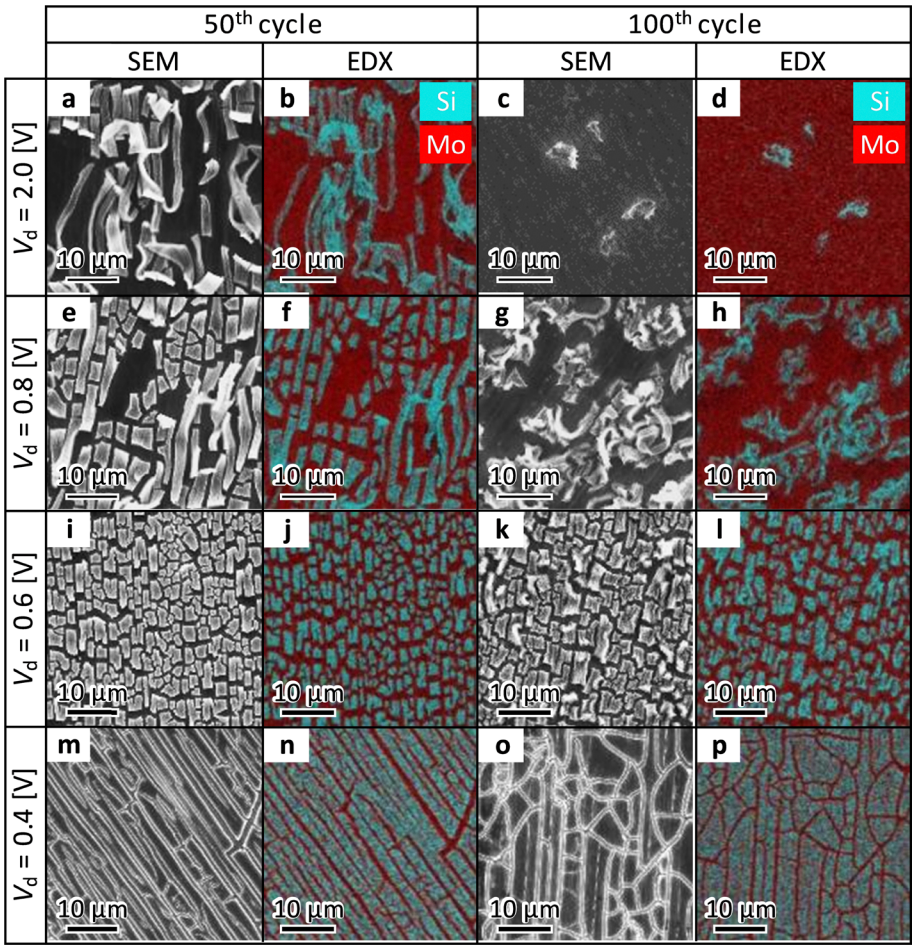


Fig. 2 SEM and EDX images of the sample surface after 50 and 100 charge/discharge cycles at different $V_d$: (a)–(d) 2.0 V, (e)–(h) 0.8 V, (i)–(l) 0.6 V, and (m)–(p) 0.4 V. In the EDX images, Si is shown in light blue and Mo in red.


© 2026 The Author(s). Published by the Royal Society of Chemistry

Open Access Article. Published on 17 December 2025. Downloaded on 4/2/2026 1:22:20 PM.
This article is licensed under a Creative Commons Attribution 3.0 Unported Licence.

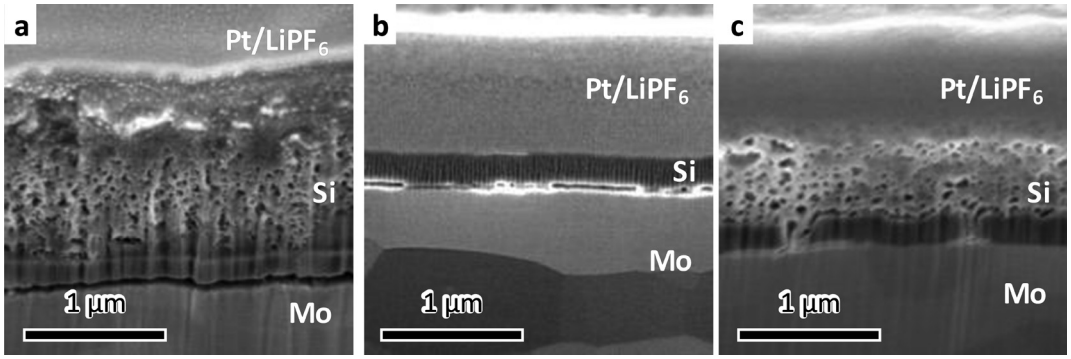


Fig. 3 Cross-sectional FIB-SEM images of the samples. (a) After 2nd charge at $V_d$ = 2.0 V. (b) and (c) After 2nd discharge at $V_d$ = (b) 2.0 V and (c) 0.6 V.

In contrast, the 0.6 V sample maintains strong and well-defined peaks up to the 100th cycle. Although slight peak shifts are observed, the overall peak shape and intensity remain largely preserved, indicating stable lithiation/delithiation pathways and suppressed polarization growth. The 0.4 V sample exhibited fewer and weaker peaks, with the peak positions shifting to lower and higher potentials during lithiation and delithiation, respectively, suggesting incomplete Li extraction. These results demonstrate that setting $V_d$ within the intermediate range of the Si–Li reaction effectively limits excessive delithiation and mitigates degradation, thereby extending the cycle life of Si anodes. Compared with previous voltage-window studies on Si-based anodes, which mainly evaluated composite or thick-film electrodes and focused on lower cut-off regulation, the present results highlight the distinct effect of controlling the upper cut-off voltage in Si thin films. The superior capacity retention at 0.6 V—together with sustained d$Q$/d$V$ features—demonstrates that partial delithiation effectively suppresses degradation, a trend not explicitly reported in earlier thin-film studies. The delithiation cut-off voltage regulation provides an additional and practical design parameter for improving the cycling durability of Si thin-film anodes.

Fig. 2 shows the SEM images and corresponding EDX maps of the Si anode surfaces after 50 and 100 cycles at different $V_d$ of 2.0, 0.8, 0.6, and 0.4 V. The charge/discharge tests were conducted at 1C, and the cells were disassembled to observe the Si surface. In all samples, cracks were observed in the Si layer, which originated from the repeated volume expansion and contraction during lithiation and delithiation. The progressive surface deterioration with cycling is consistent with the well-known mechanical failure behavior of Si anodes.[25,44] In the 2.0 V sample, delamination of the Si film was evident after 50 cycles, exposing parts of the underlying Mo substrate (Fig. 2(a) and (b)). After 100 cycles, most of the Si layer had peeled off, leaving the substrate nearly bare (Fig. 2(c) and (d)). In the 0.8 V sample, partial delamination was observed after 50 cycles; however, the remaining Si coverage was greater than that in the 2.0 V sample, and a substantial portion of the Si layer still remained after 100 cycles (Fig. 2(e)–(h)). In contrast, the 0.6 V sample retained a continuous Si layer that adhered firmly to the Mo substrate without apparent delamination. The film exhibited a finely divided morphology, likely caused by local microcrack formation rather than large-scale peeling. Even after 100 cycles, the Si layer remained intact, confirming that delamination was effectively suppressed. This morphological stability supports the excellent capacity retention observed at 0.6 V. For the 0.4 V sample, the Si layer also remained on the substrate after 100 cycles and showed less structural damage than the others. This result is attributed to the small mechanical stress caused by limited delithiation, which reduced volume change and mitigated damage to the Si film.

Fig. 3(a)–(c) presents the cross-sectional FIB-SEM images of the Si anodes after two charge/discharge cycles at 1C. In the charged state (Fig. 3(a)), the Si layer expanded significantly. Although the theoretical volume expansion of fully lithiated Si is approximately 400%,[6,11] the observed expansion appeared even larger, probably because lateral expansion was constrained by the substrate, forcing the Si layer to expand mainly in the vertical direction. A distinct gap was observed at the Si/Mo interface, suggesting that interfacial damage occurred even after only a few cycles. Additionally, the morphologies near the surface and the interface differed, indicating nonuniform Li insertion and the presence of a Li concentration gradient within the Si layer. In the discharged state at 2.0 V (Fig. 3(b)), the Si layer contracted markedly as Li ions were extracted. Such repeated expansion and contraction likely lead to the accumulation of mechanical stress, crack propagation, and eventual delamination, resulting in loss of electrode activity. In contrast, the discharged 0.6 V sample (Fig. 3(c)) did not exhibit complete contraction, suggesting incomplete delithiation. Partial retention of Li in the Si layer may relax mechanical stress at the interface, thereby suppressing damage accumulation and improving the long-term cycling stability.

Fig. 4 shows the cross-sectional TEM and EDX images of the Si anodes after two charge/discharge cycles at 1C, discharged to 2.0 and 0.6 V. In the 2.0 V sample (Fig. 4(a)–(e)), a large gap formed at the Si/substrate interface, indicating severe delamination. The EDX elemental maps revealed fluorine in this interfacial region, suggesting that electrolyte-derived species, including possible SEI components, had penetrated the gap between the Si layer and the Mo substrate. In contrast, the interfacial gap in the 0.6 V sample (Fig. 4(f)–(j)) was much smaller, and the Si layer remained closely attached to the substrate. The Si layer appeared slightly thinner than in the

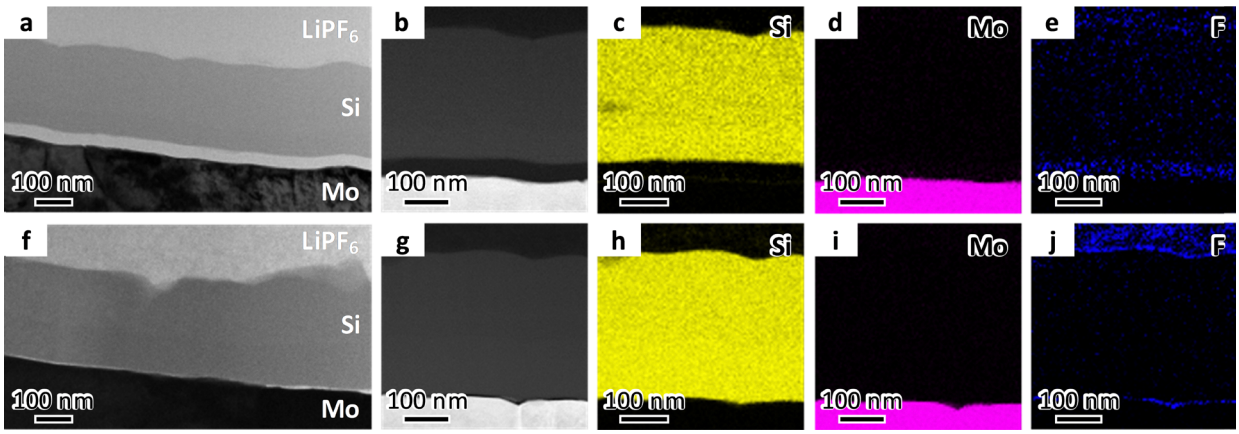


Fig. 4 Cross-sectional structures of the samples after 2nd discharge at $V_d$ = (a)–(e) 2.0 V and (f)–(j) 0.6 V. (a) and (f) Bright-field TEM images, (b) and (g) HAADF-STEM images, and EDX mappings of (c) and (h) Si, (d) and (i) Mo, and (e) and (j) F.

Open Access Article. Published on 17 December 2025. Downloaded on 4/2/2026 1:22:20 PM.
This article is licensed under a Creative Commons Attribution 3.0 Unported Licence.

FIB-SEM image of Fig. 3, likely due to spontaneous delithiation during the time between the electrochemical test and TEM observation. This delithiation induced stress relaxation, resulting in a reduced apparent thickness.[45–48] Although a thin interfacial layer was observed in some regions of the TEM images, this does not imply that the entire Si film was detached. Si thin films can maintain electrical contact even when only part of the interface remains firmly adhered, and such partial adhesion is sufficient for the anode to function. These findings suggest that controlling the delithiation cut-off voltage to avoid complete delithiation effectively suppresses excessive shrinkage of the Si layer, thereby mitigating delamination and contributing to the improved structural and electrochemical stability of the anode.

## Conclusions

The effect of delithiation cut-off voltage on the electrochemical and structural stability of Si thin-film anodes was systematically investigated. All samples showed clear charge/discharge behavior; however, the cycling performance varied markedly depending on the delithiation cut-off voltage. The 2.0 V sample exhibited rapid capacity fading and severe delamination of the Si film from the Mo substrate, whereas the 0.6 V sample maintained high capacity retention and structural integrity even after 100 cycles. Cross-sectional analyses clarified that complete delithiation caused significant contraction of the Si layer and formation of interfacial voids, while partial delithiation at 0.6 V effectively suppressed such damage. This voltage-controlled suppression of mechanical stress minimized interfacial degradation and enhanced long-term durability. Adjusting the delithiation cut-off voltage within the Si–Li reaction range enables control over Li extraction, thereby mitigating excessive shrinkage and delamination. Although this study demonstrates the effectiveness of cut-off regulation on Mo substrates, the voltage effect may vary depending on substrate stiffness and intrinsic adhesion. This study provides a new electrochemical perspective for extending the cycle life of Si-based anodes through simple potential window optimization.

## Conflicts of interest

There are no conflicts to declare.

## Data availability

Data for this article are available at Open Science Framework at https://osf.io/vznqf.

## Acknowledgements

This work was financially supported by the JSPS KAKENHI (22K18802, 25K22083) and the JST FOREST Program (JPMJFR222J). The experiments were conducted at the International Center for Young Scientists at NIMS and the Nanotechnology Platform at the University of Tsukuba.

## Notes and references

1 J. M. Tarascon and M. Armand, *Nature*, 2001, **414**, 359–367.
2 P. Parvizi, M. Jalilian, A. M. Amidi, M. R. Zangeneh and J. R. Riba, *Micromachines*, 2025, **16**, 194.
3 A. Aghmadi and O. A. Mohammed, *Batteries*, 2024, **10**, 141.
4 H. Murata, Y. Nakajima, Y. Kado, N. Saitoh, N. Yoshizawa, T. Suemasu and K. Toko, *ACS Appl. Energy Mater.*, 2020, **3**, 8410–8414.
5 T. Suzuki, H. Murata, Y. Kado, T. Ishiyama, N. Saitoh, N. Yoshizawa, T. Suemasu and K. Toko, *ACS Appl. Mater. Interfaces*, 2022, **14**, 54670–54675.
6 C. M. Park, J. H. Kim, H. Kim and H. J. Sohn, *Chem. Soc. Rev.*, 2010, **39**, 3115.
7 H. Tian, F. Xin, X. Wang, W. He and W. Han, *J. Mater.*, 2015, **1**, 153–169.
8 G. Zhu, D. Chao, W. Xu, M. Wu and H. Zhang, *ACS Nano*, 2021, **15**, 15567–15593.


© 2026 The Author(s). Published by the Royal Society of Chemistry

Open Access Article. Published on 17 December 2025. Downloaded on 4/2/2026 1:22:20 PM. This article is licensed under a Creative Commons Attribution 3.0 Unported Licence.

9 L. Y. Beaulieu, K. W. Eberman, R. L. Turner, L. J. Krause and J. R. Dahn, *Electrochem. Solid-State Lett.*, 2001, **4**, A137–A140.
10 A. Magasinski, P. Dixon, B. Hertzberg, A. Kvit, J. Ayala and G. Yushin, *Nat. Mater.*, 2010, **9**, 353–358.
11 J. R. Szczech and S. Jin, *Energy Environ. Sci.*, 2011, **4**, 56–72.
12 H. Wu and Y. Cui, *Nano Today*, 2012, **7**, 414–429.
13 M. Ge, X. Fang, J. Rong and C. Zhou, *Nanotechnology*, 2013, **24**, 422001.
14 X. Su, Q. Wu, J. Li, X. Xiao, A. Lott, W. Lu, B. W. Sheldon and J. Wu, *Adv. Energy Mater.*, 2014, **4**, 1300882.
15 M. A. Rahman, G. Song, A. I. Bhatt, Y. C. Wong and C. Wen, *Adv. Funct. Mater.*, 2016, **26**, 647–678.
16 X. Zuo, J. Zhu, P. Müller-Buschbaum and Y.-J. Cheng, *Nano Energy*, 2017, **31**, 113–143.
17 M. Zhou, X. Li, B. Wang, Y. Zhang, J. Ning, Z. Xiao, X. Zhang, Y. Chang and L. Zhi, *Nano Lett.*, 2015, **15**, 6222–6228.
18 F. Maroni, R. Raccichini, A. Birrozzi, G. Carbonari, R. Tossici, F. Croce, R. Marassi and F. Nobili, *J. Power Sources*, 2014, **269**, 873–882.
19 N. Fukata, M. Mitome, Y. Bando, W. Wu and Z. L. Wang, *Nano Energy*, 2016, **26**, 37–42.
20 X. Shen, Z. Tian, R. Fan, L. Shao, D. Zhang, G. Cao, L. Kou and Y. Bai, *J. Energy Chem.*, 2018, **27**, 1067–1090.
21 W. Chen, Y. Liao, K. Chen, R. Zeng, M. Wan, Y. Guo, J. Peng, J. Meng, L. Xue and W. Zhang, *J. Electroanal. Chem.*, 2023, **929**, 117093.
22 Ł. Kondracki, J. P. Niemela, D. Baster, M. El Kazzi, I. Utke and S. Trabesinger, *ACS Appl. Energy Mater.*, 2024, **7**, 9336–9348.
23 Q. Ai, D. Li, J. Guo, G. Hou, Q. Sun, Q. Sun, X. Xu, W. Zhai, L. Zhang, J. Feng, P. Si, J. Lou and L. Ci, *Adv. Mater. Interfaces*, 2019, **6**, 1901187.
24 B. Peng, W. Bao, K. Sun and J. Xiao, *Nanomaterials*, 2025, **15**, 690.
25 C. E. L. Foss, M. K. Talkhoncheh, A. Ulvestad, H. F. Andersen, P. E. Vullum, N. P. Wagner, K. Friestad, A. Y. Koposov, A. van Duin and J. P. Mæhlen, *J. Phys. Chem. Lett.*, 2025, **16**, 2238–2244.
26 J. Moon, H. C. Lee, H. Jung, S. Wakita, S. Cho, J. Yoon, J. Lee, A. Ueda, B. Choi, S. Lee, K. Ito, Y. Kubo, A. C. Lim, J. G. Seo, J. Yoo, S. Lee, Y. Ham, W. Baek, Y.-G. Ryu and I. T. Han, *Nat. Commun.*, 2021, **12**, 2714.
27 G. Kloker, M. Anjass, F. Brauchle, D. Rutz and D. Vrankovic, *J. Power Sources*, 2025, **652**, 237620.
28 S. D. Beattie, M. J. Loveridge, M. J. Lain, S. Ferrari, B. J. Polzin, R. Bhagat and R. Dashwood, *J. Power Sources*, 2016, **302**, 426–430.
29 A. L. Bhat, J.-K. Chang and Y.-S. Su, *Electrochim. Acta*, 2024, **481**, 143948.
30 L. Chai, X. Wang, C. Bi, B. Su, C. Zhang, X. Li and W. Xue, *ACS Appl. Energy Mater.*, 2023, **6**, 9314–9324.
31 Z. Wu, J. Tao, L. Lin, J. Wang, J. Li, S. Mathur and Y. Lin, *Carbon Neutralization*, 2025, **4**, e70052.
32 L. Tong, P. Wang, W. Fang, X. Guo, W. Bao, Y. Yang, S. Shen and F. Qiu, *ACS Appl. Mater. Interfaces*, 2020, **12**, 29242–29252.
33 M. Schmerling, J. Schwenzel and M. Busse, *Thin Solid Films*, 2018, **655**, 77–82.
34 H. Jeon, I. Cho, H. Jo, K. Kim, M.-H. Ryou and Y. M. Lee, *RSC Adv.*, 2017, **7**, 35681–35686.
35 K. Nozawa, H. Murata, T. Suemasu and K. Toko, *ACS Appl. Nano Mater.*, 2022, **5**, 16037–16043.
36 J. Sakabe, N. Ohta, T. Ohnishi, K. Mitsuishi and K. Takada, *Commun. Chem.*, 2018, **1**, 24.
37 L. Huang, M. J. Loveridge, R. Genieser, M. J. Lain and R. Bhagat, *Sci. Rep.*, 2018, **8**, 19929.
38 E. Feyzi, M. R. Anil Kumar, X. Li, S. Deng, J. Nanda and K. Zaghib, *Next Energy*, 2024, **5**, 100176.
39 H. Lin, K. Uosaki and H. Noguchi, *Appl. Surf. Sci.*, 2021, **569**, 151040.
40 R. P. Putra, K. Matsushita, T. Ohnishi and T. Masuda, *J. Phys. Chem. Lett.*, 2024, **15**, 490–498.
41 G. Kim, M.-J. Yang, S. Lee and J.-H. Shim, *Materials*, 2025, **18**, 515.
42 B. Key, R. Bhattacharyya, M. Morcrette, V. Seznec, J.-M. Tarascon and C. P. Grey, *J. Am. Chem. Soc.*, 2009, **131**, 9239–9249.
43 F. Ozanam and M. Rosso, *Mater. Sci. Eng. B*, 2016, **213**, 2–11.
44 F. Shi, Z. Song, P. N. Ross, G. A. Somorjai, R. O. Ritchie and K. Komvopoulos, *Nat. Commun.*, 2016, **7**, 11886.
45 K. W. Schroder, H. Celio, L. J. Webb and K. J. Stevenson, *J. Phys. Chem. C*, 2012, **116**, 19737–19747.
46 S.-H. Kim, K. Dong, H. Zhao, A. A. El-Zoka, X. Zhou, E. V. Woods, F. Giuliani, I. Manke, D. Raabe and B. Gault, *J. Phys. Chem. Lett.*, 2022, **13**, 8416–8421.
47 V. A. Sethuraman, M. J. Chon, M. Shimshak, V. Srinivasan and P. R. Guduru, *J. Power Sources*, 2010, **195**, 5062–5066.
48 I. Källquist, R. Le Ruyet, H. Liu, R. Mogensen, M.-T. Lee, K. Edström and A. J. Naylor, *J. Mater. Chem. A*, 2022, **10**, 19466–19505.

© 2026 The Author(s). Published by the Royal Society of Chemistry